

Extreme Eigenvalues based Detectors for Spectrum Sensing in Cognitive Radio Networks

Wenjing Zhao, Syed Sajjad Ali, Minglu Jin, Member, IEEE, Guolong Cui, Senior Member, IEEE,
Nan Zhao, Senior Member, IEEE, and Sang Jo Yoo, Member, IEEE

Abstract—This paper focuses on the design of the optimal or near-optimal detector resorting to extreme eigenvalues. A general framework for detector design involving model-driven and data-driven approaches is introduced. Specifically, the extreme eigenvalues based likelihood ratio test (LRT) is derived via the model-driven approach. Merging the model-driven and data-driven approaches, the Naive Bayesian detector is proposed based on the extreme eigenvalues, which converts the design of test statistic into a two-class decision boundary construction problem, and a solution is provided by the Naive Bayesian classifier. To render the detectors more practical, two near-optimal detectors called α -sum and α -product of maximum and minimum eigenvalues (α -SMME, α -PMME) are further designed, in which α is a weight coefficient. Furthermore, the theoretical performance analysis of the α -SMME and α -PMME algorithms is provided, and the optimal weight selection is further obtained by solving an optimization problem under the Neyman-Pearson criterion. Finally, simulation experiments demonstrate that the proposed detectors achieve performance improvements over the state-of-the-art detectors using extreme eigenvalues, and almost coincide with the detection performance of the LRT detector.

Index Terms—Cognitive radio, spectrum sensing, extreme eigenvalues.

I. INTRODUCTION

SPECTRUM resources are becoming increasingly scarce with the rapid growth of network device access, which poses great challenges to the next generation of wireless communication networks [1]-[2]. To address this issue, cognitive radio (CR) was proposed as a promising technology [3]. Spectrum sensing, which is the primary step of CR, is aimed at reusing the licensed spectrum by the secondary users (SU). To obtain this permission without interfering with the primary user (PU), the SU is required to frequently identify the occupation status of the authorized frequency band by accurately detecting the presence of the PU signal.

Manuscript received xxx, 2021; revised xxx, 2021. This work was supported by the National Natural Science Foundations of China under Grants 62101098.

W. Zhao is with School of Information and Communication Engineering, University of Electronic Science and Technology of China, Chengdu 611731, China and also with the School of Information and Communication Engineering, Dalian University of Technology, Dalian 116024, China (email: wjzhao_20_65@163.com).

S. Ali, M. Jin, and N. Zhao are with the School of Information and Communication Engineering, Dalian University of Technology, Dalian 116024, China (email: ssajjadali2002@yahoo.com, mljin@dlut.edu.cn, zhao-nan@dlut.edu.cn).

G. Cui is with School of Information and Communication Engineering, University of Electronic Science and Technology of China, Chengdu 611731, China (email: cuiguolong@uestc.edu.cn).

S. Yoo is with Department of Information and Communication Engineering, INHA University, Incheon, South Korea (email: sjyoo@inha.ac.kr).

During the past decade, many effective detection schemes based on different features have been proposed to distinguish the PU signal from noise, such as cyclostationary feature detection [4] and energy detection (ED) [5]. Due to ease of implementation and low computational complexity, the received signal energy is the commonly used feature in the open literature [6]-[8]. However, the invariant threshold of ED is difficult to obtain in the case of front-end receiver gain variations [9]-[11]. Besides, in practical scenarios, the received signals are correlated due to factors such as oversampling and multipath propagation [12]. Energy is not a suitable feature to distinguish signal from noise for the correlated signals case.

To address the problem that ED has degraded detection performance in the case for correlated signals, some detectors were designed by exploiting correlation features, such as covariance [13]-[16]. Considering that the eigenvalues of covariance matrix can capture the correlation between the received signals well, some detectors based on eigenvalues were proposed [17]-[19]. Generally, the detectors based on eigenvalues are divided into two categories according as the test statistics are generated by all eigenvalues or extreme eigenvalues (maximum and minimum eigenvalues) [20]-[21].

The typical detectors based on all eigenvalues include the maximum eigenvalue to trace (MET) detection [22]-[24], arithmetic-geometric mean (AGM) detection [25]-[26], and the ratio of maximum eigenvalue to geometric mean of all eigenvalues (MEGM) [27]. Taking full advantage of the merits of MET, AGM and MEGM, the authors of [28] proposed a fusion detection algorithm, which outperforms the three individual algorithms. The superior performance of the detector using all eigenvalues comes at the cost of high computational complexity.

Typical algorithms on the basis of extreme eigenvalues include maximum eigenvalue detection (MED) [17], minimum eigenvalue detection (MIN) [29], the difference between the maximum eigenvalue and minimum eigenvalue (DMM) detection [30], the ratio of the maximum eigenvalue to minimum eigenvalue (MME) detection [19], [31] (also referred to as the standard condition number detector [32]-[33]), and mean-to-square extreme eigenvalue (MSEE) detection [34]. Compared with the detectors based on all eigenvalues, the detectors using the extreme eigenvalues require less computational complexity [35], while retaining the main information of signal and noise. Therefore, the extreme eigenvalues are more favored features for signal detection.

The existing detectors resorting to the extreme eigenvalues show different detection performance. Compared with the

0000-0000/00\$00.00 © 2021 IEEE.

detectors using all eigenvalues, these detectors based on the extreme eigenvalues have degraded detection performance. The performance of the existing detectors based on extreme eigenvalues needs to be further improved especially in the low signal-to-noise ratio (SNR) scenarios. Although many detectors using extreme eigenvalues were proposed, to authors' knowledge, the extreme eigenvalues based optimal detector has not been devised in the open literature. Natural questions then arise: Is there a new detector based on extreme eigenvalues with even better performance and how to design the optimal detector? To deal with these two problems, we discuss the design of the optimal or near-optimal detector based on the extreme eigenvalues via different approaches.

The fundamental problem of detector design is to choose the favorable features that can capture signal and noise characteristics well, and to construct the test statistics for decision making. Model-driven (or model-based) approach has played a dominant role in the design of test statistics for many years [36]. When the model is sufficiently accurate, the detector derived from the model-driven approach is generally expected to be optimal [37]. However, the model-driven method is limited when the model is unavailable or inaccurate in complicated scenarios [37]. On the contrary, the data-driven approach independent of the powerful models is an effective tool for data analysis and feature extraction [36], which provides a new way to detector design. In this respect, this paper first summarizes a general framework for the design of spectrum sensing algorithms using model-driven or data-driven approaches. Under this framework, we discuss the design of the optimal or near-optimal detector based on extreme eigenvalues via model-driven approach and a combination of model-driven and data-driven approaches. The main contributions are summarized as below.

- In the model-driven approach, the extreme eigenvalues based likelihood ratio test (LRT) detector is derived under the Gaussian distribution approximation, which is proved to be the optimal detector according to the Neyman-Pearson criterion.
- By merging the model-driven and data-driven approaches, a Naive Bayesian (NB) detector is devised on the basis of the extreme eigenvalues, where the design of test statistic is regarded as the problem of constructing a two-class decision boundary in the feature domain, and a solution is given by the Naive Bayesian classifier.
- To render the detectors more practical, two extreme eigenvalues based methods with simple controllable parameters are proposed, namely α -sum and α -product of maximum and minimum eigenvalues (α -SMME, α -PMME) detection, in which α is weight coefficient. Under the Neyman-Pearson criterion, the optimum weights of α -SMME and α -PMME are determined by solving the corresponding optimization problems.
- The analytical expressions for the false alarm probability, detection probability, and thresholds of α -SMME and α -PMME are derived using the Gaussian distribution approximation approach. Simulation results show that the proposed detectors outperform the state-of-the-art detec-

tors using extreme eigenvalues. Besides, the performance of the α -SMME and α -PMME detectors almost coincides with that of the LRT detector.

The remainder of this paper is structured as below. The problem formulation is introduced in Section II. Section III considers the detectors design using extreme eigenvalues. Specifically, a general design framework for spectrum sensing algorithms is first summarized; several algorithms based on extreme eigenvalues are designed through model-driven approach and merging model-driven and data-driven approaches. In Section IV, the theoretical performance analysis on the α -SMME and α -PMME algorithms is presented with the aid of Gaussian distribution, and the optimal weight α is provided. Section V discusses the performance of the proposed algorithms through simulation experiments. The last section comes to some conclusions.

II. PROBLEM FORMULATION

As shown in Fig. 1, this paper considers the typical scenario in the CR system that consists of P PUs and one SU, where each PU is equipped with a single antenna and SU is equipped with M antennas [19], [21]. In the CR network, the SU periodically identifies the occupation status of the authorized frequency band. If the PU does not occupy the current frequency band, then the SU can access the current frequency band; otherwise, the SU is not allowed to access this licensed frequency band.

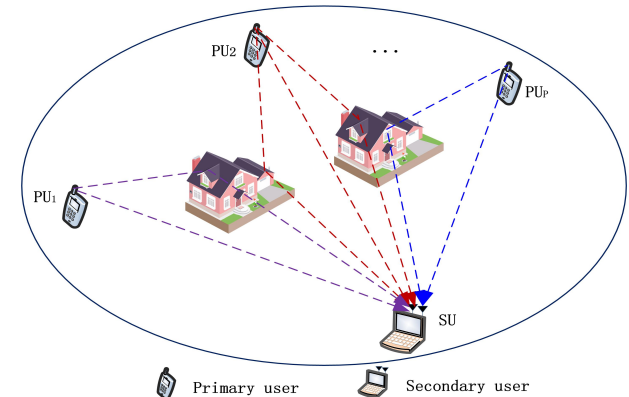


Fig. 1. Typical scenario in the CR system.

Let $x_m(k)$ be the received discrete-time sample from the m -th receiving antenna of SU, where $m = 1, \dots, M$ denotes the antenna index, and $k = 0, \dots, K - 1$ denotes the time (sample) index. Specifically, $x_m(k)$ is given by

$$\begin{cases} H_0 : x_m(k) = w_m(k), \\ H_1 : x_m(k) = \sum_{p=1}^P \sum_{l=0}^{C_{mp}} h_{mp}(l)s_p(k-l) + w_m(k), \end{cases} \quad (1)$$

where H_0 represents the PU signal is absent under null hypothesis, and H_1 represents the PU signal is present under alternative hypothesis; $s_p(k)$ denotes the k -th sample of the p -th PU signal; $h_{mp}(l)$ denotes the propagation channel from the p -th PU to the m -th antenna at the SU terminal, l denotes the delay lag variable, and $l = 0$ indicates the line-of-sight

path, C_{mp} is the order of channel $h_{mp}(l)$ [19]; $w_m(k)$ is the additive Gaussian noise at the m -th receiving antenna, and it is modeled as a circularly symmetric complex Gaussian variable with zero mean and variance σ_w^2 . Without loss of generality, noise and signal are assumed to be statistically independent of each other. It is noted that the model in (1) is also applicable to multiple single-antenna receivers case where $x_m(k)$ becomes the received signal at the m -th receiver [19].

The received signal vector at the antenna array is obtained by putting together the received samples at one time instant. For the case of H_1 , let $C_p = \max_m C_{mp}$, the received signal vector is specifically described as

$$\mathbf{x}(k) = \sum_{p=1}^P \sum_{l=0}^{C_p} \mathbf{h}_p(l) s_p(k-l) + \mathbf{w}(k), \quad (2)$$

where

$$\begin{cases} \mathbf{x}(k) = [x_1(k), \dots, x_M(k)]^T, \\ \mathbf{w}(k) = [w_1(k), \dots, w_M(k)]^T, \\ \mathbf{h}_p(l) = [h_{1p}(l), \dots, h_{Mp}(l)]^T, \end{cases} \quad (3)$$

in which superscript $(\cdot)^T$ indicates transpose.

For notational simplicity, let $\tilde{\mathbf{s}}(k) = \sum_{p=1}^P \sum_{l=0}^{C_p} \mathbf{h}_p(l) s_p(k-l)$ be the received source signal, which includes the effects of path loss and multipath fading. The received signal vector under H_1 is simplified as

$$\mathbf{x}(k) = \tilde{\mathbf{s}}(k) + \mathbf{w}(k). \quad (4)$$

For the received signal in (4), the average received SNR is defined as the ratio of the average received source signal power to the average noise power [19], which is given by

$$\text{SNR} \stackrel{\text{def}}{=} \frac{E(\|\tilde{\mathbf{s}}(k)\|^2)}{E(\|\mathbf{w}(k)\|^2)}, \quad (5)$$

where $E(\cdot)$ is the expectation operator and $\|\cdot\|$ represents the vector 2-norm.

According to (4), the vector form of equation (1) is given by

$$\begin{cases} H_0 : \mathbf{x}(k) = \mathbf{w}(k), \\ H_1 : \mathbf{x}(k) = \tilde{\mathbf{s}}(k) + \mathbf{w}(k). \end{cases} \quad (6)$$

The sample covariance matrix generated by K received signal vectors in (6) is formulated as

$$\hat{\mathbf{R}}_{\mathbf{x}}(K) = \frac{1}{K} \sum_{k=0}^{K-1} \mathbf{x}(k) \mathbf{x}^H(k), \quad (7)$$

where $(\cdot)^H$ denotes conjugate transpose. If the current frequency band is utilized by the PU, then the covariance matrix structure is different from the case where the frequency band is free. Generally, the eigenvalues can well extract the main information and correlation of data. Therefore, the eigenvalues of covariance matrix are widely considered as popular features for designing powerful detectors.

III. DETECTORS DESIGN ON THE BASIS OF EXTREME EIGENVALUES

A. A General Design Framework for Spectrum Sensing Algorithms

This paper first summarizes a general framework for the design of spectrum sensing algorithms. As shown in Fig. 2, the framework is built on the signal space, feature space and decision space. The mapping from the signal space to the feature space is referred to as transformation block, which transforms the received data into different features. The mapping from the feature space to the decision space is referred to as computation block, which generates test statistics from features. Finally, the decision result is obtained by comparing the test statistic with threshold η .

The transformation block and computation block can be devised via model-driven or data-driven approaches. In the model-driven approach, the transformation block and computation block depend on a signal model (or probability model) [37]. The model-driven approach is utilized when the statistical characteristics of the signal or feature are known or easily available. For example, the existing algorithms based on eigenvalues are designed through model-driven approach. However, the model-driven approach is limited by model accuracy, on the contrary, the data-driven approach does not depend on the powerful models [36]. Data-driven approach, which is a powerful tool for data analysis and feature extraction, provides a new perspective for designing detectors. The data-driven approach can be exploited when the sufficient data sets are available. Based on the above analysis, the design approaches for transformation block and computation block are divided into four categories. In this paper, we study the optimal detector design on the feature space composed of the maximum eigenvalue and minimum eigenvalue. Since the feature space is fixed, the following subsections probe into the detector design by devising the computation block via the model-driven or data-driven approaches.

B. Extreme Eigenvalues based Detectors Design Using Model-driven Approach

This subsection briefly reviews the existing algorithms resorting to the extreme eigenvalues, and designs the optimal detector based on the extreme eigenvalues via a model-driven approach. The test statistics of the existing detectors based on extreme eigenvalues are summarized in Table I, where $\lambda_1(\hat{\mathbf{R}}_{\mathbf{x}}(K))$ and $\lambda_M(\hat{\mathbf{R}}_{\mathbf{x}}(K))$ represent the maximum eigenvalue and minimum eigenvalue of the sample covariance matrix $\hat{\mathbf{R}}_{\mathbf{x}}(K)$ in (7). Under the framework in Fig. 2, the algorithms in Table I can be designed by using $\lambda_1(\hat{\mathbf{R}}_{\mathbf{x}}(K))$ and $\lambda_M(\hat{\mathbf{R}}_{\mathbf{x}}(K))$ as the features. The difference among these algorithms lies in the computation of test statistics. These detectors resorting to different test statistics show different detection performance.

According to the Neyman-Pearson criterion, the LRT detector is the optimal solution to the problem in (1). To authors' knowledge, there is no related work to derive the LRT detector based on the extreme eigenvalues in the model-driven approach. Motivated by this, we investigate the design

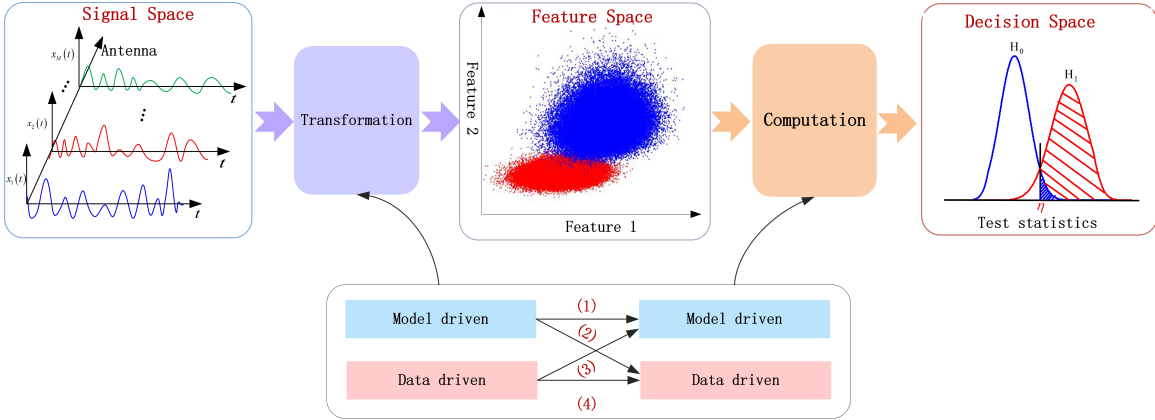


Fig. 2. General design framework for spectrum sensing algorithms.

TABLE I
TEST STATISTICS FOR THE EXISTING DETECTORS USING EXTREME EIGENVALUES.

Name	MED [17]	MIN [29]	DMM [30]	MME [31]	MSEE [34]
Test statistics	$\lambda_1(\hat{\mathbf{R}}_{\mathbf{x}}(K))$	$\lambda_M(\hat{\mathbf{R}}_{\mathbf{x}}(K))$	$\lambda_1(\hat{\mathbf{R}}_{\mathbf{x}}(K)) - \lambda_M(\hat{\mathbf{R}}_{\mathbf{x}}(K))$	$\frac{\lambda_1(\hat{\mathbf{R}}_{\mathbf{x}}(K))}{\lambda_M(\hat{\mathbf{R}}_{\mathbf{x}}(K))}$	$\frac{\frac{1}{2}(\lambda_1(\hat{\mathbf{R}}_{\mathbf{x}}(K)) + \lambda_M(\hat{\mathbf{R}}_{\mathbf{x}}(K)))}{(\lambda_1(\hat{\mathbf{R}}_{\mathbf{x}}(K))\lambda_M(\hat{\mathbf{R}}_{\mathbf{x}}(K)))^{\frac{1}{2}}}$

of the optimal LRT detector with the aid of the statistical distributions of the extreme eigenvalues.

The joint distribution of two extreme eigenvalues was studied in [38]-[41]. Using moment matching method, the authors of [42] demonstrated that the bivariate Gaussian distribution function can approximate the joint probability density function (PDF) of two extreme eigenvalues well. The joint PDFs of λ_1 and λ_M under H_0 and H_1 are respectively given by [42]

$$f_{\lambda_1, \lambda_M}^{H_0}(x, y) = \frac{1}{2\pi\sigma_{\lambda_1, H_0}\sigma_{\lambda_M, H_0}(1-\rho_0^2)^{0.5}} \exp\left(-\frac{\kappa_0}{2(1-\rho_0)^2}\right), \quad (8)$$

and

$$f_{\lambda_1, \lambda_M}^{H_1}(x, y) = \frac{1}{2\pi\sigma_{\lambda_1, H_1}\sigma_{\lambda_M, H_1}(1-\rho_1^2)^{0.5}} \exp\left(-\frac{\kappa_1}{2(1-\rho_1)^2}\right), \quad (9)$$

where κ_0 and κ_1 are expressed as

$$\kappa_i = \frac{(x - \mu_{\lambda_1}^{H_i})^2 - 2\rho_i(x - \mu_{\lambda_1}^{H_i})(y - \mu_{\lambda_M}^{H_i}) + (y - \mu_{\lambda_M}^{H_i})^2}{\sigma_{\lambda_1, H_i}^2 + \sigma_{\lambda_M, H_i}^2}, \quad i=0, 1, \quad (10)$$

in which $\mu_{\lambda_1}^{H_i}$ and $\mu_{\lambda_M}^{H_i}$ are the mean of λ_1 and λ_M for the case of H_i ; $\sigma_{\lambda_1, H_i}^2$ and $\sigma_{\lambda_M, H_i}^2$ are the variance of λ_1 and λ_M under H_i ; ρ_0 and ρ_1 are the correlation coefficients between λ_1 and λ_M under H_0 and H_1 , respectively.

Based on (8) and (9), the test statistic of the LRT detector in regard to λ_1 and λ_M is obtained

$$L(\lambda_1, \lambda_M) = \frac{f_{\lambda_1, \lambda_M}^{H_1}(x, y)}{f_{\lambda_1, \lambda_M}^{H_0}(x, y)} = \frac{\sigma_{\lambda_1, H_0}\sigma_{\lambda_M, H_0}(1-\rho_0^2)^{0.5}}{\sigma_{\lambda_1, H_1}\sigma_{\lambda_M, H_1}(1-\rho_1^2)^{0.5}} \exp\left(-\frac{\kappa_1}{2(1-\rho_1)^2} + \frac{\kappa_0}{2(1-\rho_0)^2}\right). \quad (11)$$

Taking logarithm on (11), the test statistic of the LRT is converted into

$$\begin{aligned} \tilde{L}(\lambda_1, \lambda_M) &= \log\left(\frac{\sigma_{\lambda_1, H_0}\sigma_{\lambda_M, H_0}(1-\rho_0^2)^{0.5}}{\sigma_{\lambda_1, H_1}\sigma_{\lambda_M, H_1}(1-\rho_1^2)^{0.5}}\right) \\ &+ \frac{1}{2(1-\rho_0)^2} \left(\frac{\lambda_1 - \mu_{\lambda_1}^{H_0}}{\sigma_{\lambda_1, H_0}} - \frac{\lambda_M - \mu_{\lambda_M}^{H_0}}{\sigma_{\lambda_M, H_0}} \right)^2 + \frac{1}{(1-\rho_0)} \frac{(\lambda_1 - \mu_{\lambda_1}^{H_0})(\lambda_M - \mu_{\lambda_M}^{H_0})}{\sigma_{\lambda_1, H_0}\sigma_{\lambda_M, H_0}} \\ &- \frac{1}{2(1-\rho_1)^2} \left(\frac{\lambda_1 - \mu_{\lambda_1}^{H_1}}{\sigma_{\lambda_1, H_1}} - \frac{\lambda_M - \mu_{\lambda_M}^{H_1}}{\sigma_{\lambda_M, H_1}} \right)^2 - \frac{1}{(1-\rho_1)} \frac{(\lambda_1 - \mu_{\lambda_1}^{H_1})(\lambda_M - \mu_{\lambda_M}^{H_1})}{\sigma_{\lambda_1, H_1}\sigma_{\lambda_M, H_1}}, \end{aligned} \quad (12)$$

where $\tilde{L}(\lambda_1, \lambda_M)$ represents the log-likelihood ratio test (log-LRT) with respect to λ_1 and λ_M .

For the log-LRT detector, the decision is made by comparing the test statistic (12) with threshold, which is expressed as

$$\tilde{L}(\lambda_1, \lambda_M) \stackrel{H_1}{\gtrless} \stackrel{H_0}{\lesssim} \eta, \quad (13)$$

where η is the decision threshold.

For simplification, the constant term $\log\left(\frac{\sigma_{\lambda_1, H_0}\sigma_{\lambda_M, H_0}(1-\rho_0^2)^{0.5}}{\sigma_{\lambda_1, H_1}\sigma_{\lambda_M, H_1}(1-\rho_1^2)^{0.5}}\right)$ in (12) is merged to the threshold η . Hence, the test statistic of log-LRT detector is equivalently given by

$$\begin{aligned} \tilde{L}(\lambda_1, \lambda_M) &= \frac{1}{2(1-\rho_0)^2} \left(\frac{\lambda_1 - \mu_{\lambda_1}^{H_0}}{\sigma_{\lambda_1, H_0}} - \frac{\lambda_M - \mu_{\lambda_M}^{H_0}}{\sigma_{\lambda_M, H_0}} \right)^2 + \frac{1}{(1-\rho_0)} \frac{(\lambda_1 - \mu_{\lambda_1}^{H_0})(\lambda_M - \mu_{\lambda_M}^{H_0})}{\sigma_{\lambda_1, H_0}\sigma_{\lambda_M, H_0}} \\ &- \frac{1}{2(1-\rho_1)^2} \left(\frac{\lambda_1 - \mu_{\lambda_1}^{H_1}}{\sigma_{\lambda_1, H_1}} - \frac{\lambda_M - \mu_{\lambda_M}^{H_1}}{\sigma_{\lambda_M, H_1}} \right)^2 - \frac{1}{(1-\rho_1)} \frac{(\lambda_1 - \mu_{\lambda_1}^{H_1})(\lambda_M - \mu_{\lambda_M}^{H_1})}{\sigma_{\lambda_1, H_1}\sigma_{\lambda_M, H_1}}. \end{aligned} \quad (14)$$

As observed from (14), the log-LRT detector depends on the mean, variance and correlation coefficients of the extreme eigenvalues. When the statistical distributions of extreme eigenvalues are unavailable or biased in a complicated situation, the performance of the log-LRT detector is degraded in practical applications.

C. Extreme Eigenvalues based Detectors Design Combining Model-driven and Data-driven Approaches

The performance of all model-based detectors is limited by model accuracy. To break this limitation, this subsection probes into the detector design by merging model-driven and data-driven approaches. Specifically, our rationale is rooted in the fact that signal detection is a classification problem. In this paper, the extreme eigenvalues are the considered features, which are obtained via model-driven approaches instead of data-driven networks. In view of the fact that the decision boundary of classification corresponds to the equation in which the detection statistic is equal to the decision threshold, the design of test statistic is converted into the problem of constructing a two-class decision boundary in the feature domain, which can be implemented through a powerful classifier (data-driven approach).

The Naive Bayesian (NB) classifier is adopted in this paper due to its lower computational complexity compared to other classifiers based on probability theory. The NB classifier leverages the Bayes' theorem, which is given by

$$P_r(H_i | f_1, f_2) = \frac{P_r(f_1, f_2 | H_i) P_r(H_i)}{P_r(f_1, f_2)}, i = 0, 1, \quad (15)$$

where f_1 and f_2 represent the used features, $P_r(\cdot)$ represents the probability of an event, $P_r(H_i | f_1, f_2)$, $P_r(f_1, f_2 | H_i)$ and $P_r(H_i)$ respectively stand for the posterior probability, likelihood function and prior probability. For tractability, NB classifier assumes that f_1 and f_2 are independent of each other. The NB classifier performs well even when the assumption is not valid [43]. Hence, this paper also follows this assumption. In this paper, f_1 and f_2 correspond to the maximum eigenvalue and minimum eigenvalue.

The NB algorithm classifies data by maximizing the posterior probability, which is expressed as

$$\max_{H_i} P_r(H_i) P_r(\lambda_1 | H_i) P_r(\lambda_M | H_i). \quad (16)$$

The prior probability $P_r(H_i)$, likelihood function $P_r(\lambda_1 | H_i)$ and $P_r(\lambda_M | H_i)$ are estimated with the balanced training set in the training process. Let n_i be the number of data with class label H_i , n_t be the training set size, $\{(\lambda_1^{(d)}, \lambda_M^{(d)}, l^{(d)})\}$ be the d -th element in the training set, in which $(\lambda_1^{(d)}, \lambda_M^{(d)})$ is the feature, and $l^{(d)}$ is the corresponding label. Note that this paper does not consider the case where the sample number of a certain type is 0. $P_r(H_i)$ is given by $P_r(H_i) = \frac{n_i}{n_t}$. For $P_r(\lambda_1 | H_i)$ and $P_r(\lambda_M | H_i)$, the authors of [38] validated that the Gaussian distributions can fit the statistical distributions of λ_1 and λ_M well. Hence, this approximation is also exploited in this paper. The mean $\mu_{\lambda_j}^{H_i}$ and variance $\sigma_{\lambda_j, H_i}^2$ of the two extreme eigenvalues are estimated by

$$\hat{\mu}_{\lambda_j}^{H_i} = \frac{\sum_d \lambda_j^{(d)} U(l^{(d)} = H_i)}{\sum_d U(l^{(d)} = H_i)}, i = 0, 1, j = 1, M, \quad (17)$$

and

$$\hat{\sigma}_{\lambda_j, H_i}^2 = \frac{\sum_d \left(\lambda_j^{(d)} - \hat{\mu}_{\lambda_j}^{H_i} \right)^2 U(l^{(d)} = H_i)}{\sum_d U(l^{(d)} = H_i)}, i = 0, 1, j = 1, M, \quad (18)$$

where $U(l^{(d)} = H_i)$ is a function with binary output. If $l^{(d)} = H_i$, then $U(l^{(d)} = H_i)$ is equal to 1; otherwise, it is equal to 0.

To show the performance of the NB detector through visualization, the decision region boundaries of the NB, MED, MME, DMM and MSEE detectors are depicted in Fig. 3, where the red scatterplot and blue scatterplot respectively represent the maximum eigenvalue (λ_1) and minimum eigenvalue (λ_M) under H_0 and H_1 . Each cluster has 10,000 points under H_0 and H_1 . Under H_1 , the PU signal with -15dB is generated.

As shown in Fig. 3, MED, MME, DMM and MSEE are linear classifiers. In contrast, the NB has a nonlinear decision region boundary, which corresponds to a nonlinear classifier. According to the Neyman Pearson criterion, a good classifier should divide as many points in H_1 cluster as possible into the H_1 category (corresponding to a high detection probability), and divide fewer points in H_0 cluster into the H_1 category (corresponding to a low false alarm probability). Compared with the MED, MME, DMM and MSEE algorithms, the NB algorithm classifies fewer points in H_0 cluster or H_1 cluster into the opposite category. Hence, the NB algorithm achieves superior performance to the MED, MME, DMM and MSEE algorithms.

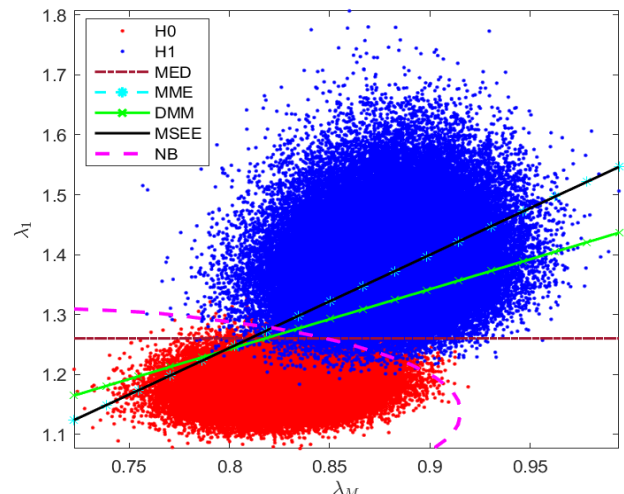


Fig. 3. Classification effects of the NB detector and some existing detectors based on extreme eigenvalues.

Compared with the existing algorithms based on extreme eigenvalues, the NB detector is time-consuming owing to training. Moreover, the decision region boundary of NB is obtained by a curve fitting method with multiple parameters. To render the detector more practical, we probe into the design of a detector with simple controllable parameters and superior performance.

First, a linear classifier with controllable parameters is considered. The test statistic is formed by the weighted sum of

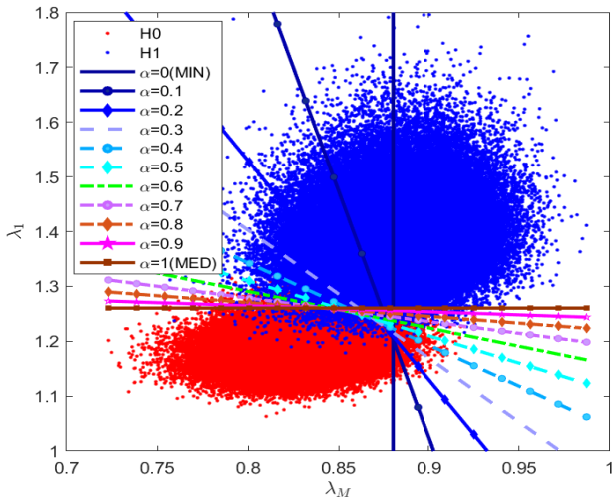


Fig. 4. Decision boundaries of the α -SMME algorithm under different α .

the maximum and minimum eigenvalues (α -SMME), which is given by

$$T_{\alpha-SMME} = \alpha \lambda_1 + (1 - \alpha) \lambda_M, \quad \alpha \in [0, 1], \quad (19)$$

where α is the weight coefficient.

From (19), it is noted that the α -SMME algorithm respectively becomes the MED algorithm and MIN algorithm for the cases of $\alpha = 1$ and $\alpha = 0$. To analyze the detection performance of the α -SMME algorithm, the decision boundaries of the α -SMME algorithm under different α are shown in Fig. 4, in which α takes a value from 0 to 1 at intervals of 0.1. As observed from Fig. 4, the α -SMME algorithm shows different classification effects under different α . For $0.5 \leq \alpha \leq 0.9$, α -SMME is more suitable for distinguishing signal from noise compared with the MED and MIN algorithms.

The results in Fig. 3 indicate that the nonlinear classifier may be a more refined detector than the linear classifier. Motivated by this, we consider the design of a nonlinear classifier. The design of the nonlinear classifier is to first perform nonlinear transformation on the features and then adopt linear classification. For simplicity, the logarithmic transformation is considered in this paper. The weighted sum operation is performed on the logarithmic transformations of the maximum and minimum eigenvalues, which is formulated as

$$\alpha \ln(\lambda_1) + (1 - \alpha) \ln(\lambda_M) = \ln(\lambda_1^\alpha \lambda_M^{1-\alpha}), \quad \alpha \in [0, 1]. \quad (20)$$

Since the natural logarithm function $\ln(\cdot)$ is a monotonically increasing function, the detector designed by (20) should show same performance as the detector with the following formula

$$T_{\alpha-PMME} = \lambda_1^\alpha \lambda_M^{1-\alpha}, \quad (21)$$

where α ranges from 0 to 1. The formula (21) is the weighted geometric mean of the maximum eigenvalue and minimum eigenvalue. For simplicity, the algorithm based on the α -product of the maximum eigenvalue and minimum eigenvalue is denoted as α -PMME. As observed from (21), α -PMME also includes the MED and MIN algorithms as special cases. The test statistic is a nonlinear function of λ_1 and λ_M , which corresponds to a nonlinear classifier. Fig. 5 shows the

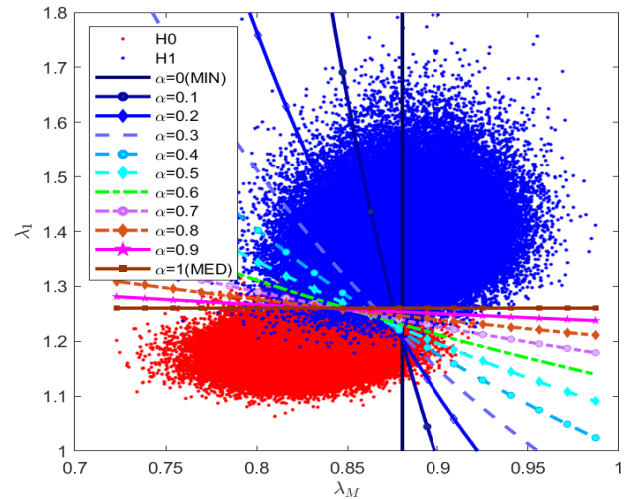


Fig. 5. Decision boundaries of the α -PMME algorithm under different α .

classification effects of the α -PMME algorithm under different α .

The deflection coefficient is exploited to further judge algorithm performance, which is given by [44]

$$\varrho^2 = \frac{(E[\xi]_{H_1} - E[\xi]_{H_0})^2}{Var[\xi]_{H_0}}, \quad (22)$$

where ξ is test statistic, $E[\xi]_{H_0}$ and $E[\xi]_{H_1}$ respectively represent the mean of ξ under H_0 and H_1 , $Var[\xi]_{H_0}$ is the variance of ξ under H_0 . A large value of ϱ^2 leads to easier distinction between the corresponding two hypotheses and results in a better detection performance [45]-[46].

Table II presents the deflection coefficients of the α -SMME and α -PMME algorithms under different α . It can be found that the α -SMME and α -PMME algorithms achieve the largest deflection coefficient when α is 0.5 and 0.6, respectively. The results indicate that α -SMME and α -PMME have superior performance when α is 0.5 and 0.6, which is consistent with the results of subsequent theoretical analysis and simulation experiments.

IV. PERFORMANCE ANALYSIS

Gaussian distribution can approximate the statistical distributions of the maximum eigenvalue and minimum eigenvalue well [38]. Under this approximation, the probability of false alarm (P_{fa}), probability of detection (P_d) and thresholds of the α -SMME and α -PMME algorithms are analyzed in this section. Besides, the optimal weights in the α -SMME and α -PMME algorithms are given under the Neyman-Pearson criterion. Finally, the computational complexity is analyzed.

A. Performance Analysis under Gaussian Distribution Approximation Approach

The dependency between λ_1 and λ_M is analyzed by using Copula (see Appendix for details). For tractability, as discussed in [47], this paper considers the simple case in which λ_1 and λ_M are independent of each other. Since the Gaussian distribution is widely employed in distribution fitting

TABLE II
DEFLECTION COEFFICIENTS OF THE α -SMME AND α -PMME ALGORITHMS UNDER DIFFERENT α

$\frac{\varrho^2}{\alpha}$	0	0.1	0.2	0.3	0.4	0.5	0.6	0.7	0.8	0.9	1
Methods											
α -SMME	14.5077	29.1889	38.4152	53.0786	59.2830	60.0118	59.7595	57.2914	54.8076	54.1008	52.4208
α -PMME	14.5077	26.7930	34.925	53.2451	55.5993	59.5267	60.7248	59.8355	57.2798	54.5498	52.4208

of positive random variables, and the Gaussian distribution function is simple and tractable, it is utilized to approximate the statistical distribution of λ_1 and λ_M in this paper. The PDFs of λ_1 and λ_M under H_0 and H_1 are given by

$$f(\lambda_i | H_i) = \frac{1}{\sqrt{2\pi}\sigma_{\lambda_i, H_i}} \exp\left(-\frac{(\lambda_i - \mu_{\lambda_i}^{H_i})^2}{2\sigma_{\lambda_i, H_i}^2}\right), i=0,1, \quad (23)$$

and

$$f(\lambda_M | H_i) = \frac{1}{\sqrt{2\pi}\sigma_{\lambda_M, H_i}} \exp\left(-\frac{(\lambda_M - \mu_{\lambda_M}^{H_i})^2}{2\sigma_{\lambda_M, H_i}^2}\right), i=0,1, \quad (24)$$

where $\mu_{\lambda_i}^{H_i}$ and $\mu_{\lambda_M}^{H_i}$ are the mean of λ_1 and λ_M for the case of H_i ; $\sigma_{\lambda_i, H_i}^2$ and $\sigma_{\lambda_M, H_i}^2$ are the variance of λ_1 and λ_M under H_i .

For any two Gaussian random variables, the linear combination of the two variables still obeys Gaussian distribution. Hence, the test statistic of the α -SMME algorithm follows the Gaussian distribution, i.e., $T_{\alpha-\text{SMME}, H_i} \sim \mathcal{N}(\mu_{\text{SMME}}^{H_i}, \sigma_{\text{SMME}, H_i}^2)$, $i = 0, 1$. The mean and variance for the test statistic of α -SMME are given by

$$\begin{cases} \mu_{\text{SMME}}^{H_i} = \alpha\mu_{\lambda_1}^{H_i} + (1-\alpha)\mu_{\lambda_M}^{H_i}, i = 0, 1, \\ \sigma_{\text{SMME}, H_i}^2 = \alpha^2\sigma_{\lambda_1, H_i}^2 + (1-\alpha)^2\sigma_{\lambda_M, H_i}^2, i = 0, 1. \end{cases} \quad (25)$$

Generally, the theoretical analysis of the algorithm involves the cumulative distribution function (CDF) of test statistic. To illustrate the effectiveness of using Gaussian distributions to approximate the statistical distributions of λ_1 , λ_M and $T_{\alpha-\text{SMME}}$, the CDF curves corresponding to the empirical results and Gaussian approximation results are shown in Fig. 6, where ‘Empirical’ and ‘Approx’ respectively represent the empirical result and approximate result. Fig. 6(a) and Fig. 6(b) respectively plot the CDF curves of λ_1 , λ_M and $T_{\alpha-\text{SMME}}$ under $K = 50$ and $K = 1000$. As observed from Fig. 6, the empirical CDFs and approximate CDFs of each statistic are almost overlapping for different values of K , which indicates the validity of approximation.

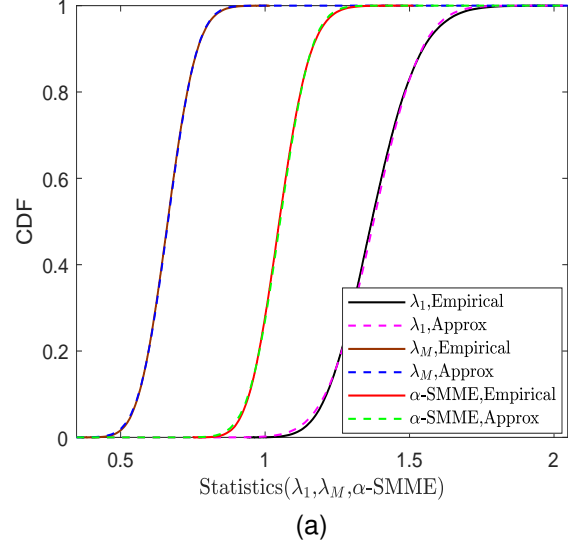
The P_{fa} of α -SMME is derived using the Gaussian distribution. In general, P_{fa} is defined by

$$P_{fa} = P_r(H_1 | H_0) = P_r(\xi > \eta | H_0), \quad (26)$$

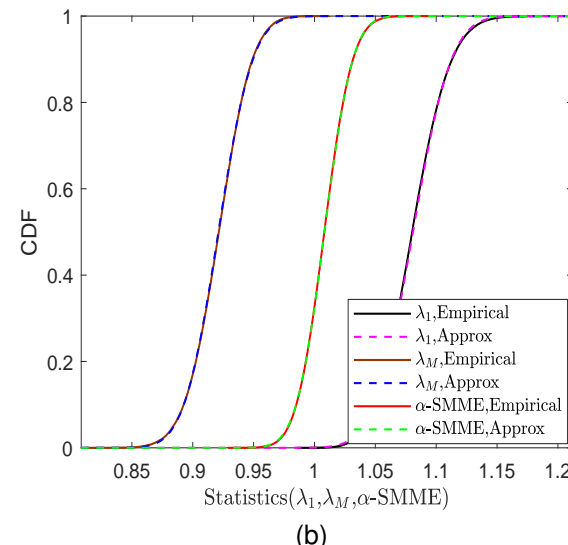
in which ξ is test statistic, and η represents threshold.

According to (25) and (26), the P_{fa} of α -SMME is expressed as

$$P_{fa}^{\text{SMME}} = \frac{1}{\sqrt{2\pi}\sigma_{\text{SMME}, H_0}^2} \int_{\eta_{\text{SMME}}}^{\infty} \exp\left(-\frac{(T_{\alpha-\text{SMME}} - \mu_{\text{SMME}}^{H_0})^2}{2\sigma_{\text{SMME}, H_0}^2}\right) dT_{\alpha-\text{SMME}}, \quad (27)$$



(a)



(b)

Fig. 6. Cumulative distribution functions for λ_1 , λ_M and the test statistic of the α -SMME algorithm. (a) $K = 50$. (b) $K = 1000$.

where η_{SMME} is decision threshold of the α -SMME algorithm. P_{fa}^{SMME} is further derived

$$P_{fa}^{\text{SMME}} = Q\left(\frac{\eta_{\text{SMME}} - \mu_{\text{SMME}}^{H_0}}{\sigma_{\text{SMME}, H_0}}\right), \quad (28)$$

in which $Q(\cdot)$ represents the complementary CDF of standard normal distribution.

The decision threshold of α -SMME is derived from (28), which is given by

$$\eta_{\text{SMME}} = Q^{-1}(P_{fa}^{\text{SMME}}) \sigma_{\text{SMME}, H_0} + \mu_{\text{SMME}}^{H_0}, \quad (29)$$

where $\mu_{\text{SMME}}^{H_0}$ and $\sigma_{\text{SMME}, H_0}$ are expressed in (25).

Under H_1 , the detection probability of α -SMME is analyzed. Generally, P_d is given by

$$P_d = P_r(H_1 | H_1) = P_r(\xi > \eta | H_1). \quad (30)$$

The P_d of α -SMME is derived on the basis of the definition in (30),

$$\begin{aligned} P_d^{\text{SMME}} &= \frac{1}{\sqrt{2\pi\sigma_{\text{SMME},H_1}^2}} \int_{\eta_{\text{SMME}}}^{\infty} \exp\left(-\frac{(T_{\alpha-\text{SMME}} - \mu_{\text{SMME}}^{H_1})^2}{2\sigma_{\text{SMME},H_1}^2}\right) dT_{\alpha-\text{SMME}} \\ &= Q\left(\frac{\eta_{\text{SMME}} - (\alpha\mu_1^{H_1} + (1-\alpha)\mu_M^{H_1})}{\sqrt{\alpha^2\sigma_{\lambda_1,H_1}^2 + (1-\alpha)^2\sigma_{\lambda_M,H_1}^2}}\right). \end{aligned} \quad (31)$$

Next we discuss the P_{fa} , threshold and P_d of the α -PMME algorithm. The formula in (20) implies

$$P_r(\ln(\lambda_1^\alpha \lambda_M^{1-\alpha}) > \eta | H_i) = P_r(\alpha \ln(\lambda_1) + (1-\alpha) \ln(\lambda_M) > \eta | H_i). \quad (32)$$

Since $\ln(\cdot)$ is a monotonically increasing function, the following relationship is satisfied

$$P_r(\ln(\lambda_1^\alpha \lambda_M^{1-\alpha}) > \eta | H_i) = P_r(\lambda_1^\alpha \lambda_M^{1-\alpha} > \exp(\eta) | H_i). \quad (33)$$

According to (32) and (33), we have

$$P_r(\alpha \ln(\lambda_1) + (1-\alpha) \ln(\lambda_M) > \eta | H_i) = P_r(\lambda_1^\alpha \lambda_M^{1-\alpha} > \exp(\eta) | H_i). \quad (34)$$

Hence, the performance analysis of the α -PMME algorithm is transformed into that of the algorithm designed for the test statistic $\alpha \ln(\lambda_1) + (1-\alpha) \ln(\lambda_M)$. For convenience, let $L\text{-}\alpha\text{-PMME} = \alpha \ln(\lambda_1) + (1-\alpha) \ln(\lambda_M)$, which denotes the logarithmic transformation of the test statistic of the α -PMME algorithm. Before delving into the P_{fa} and P_d of this algorithm, we first discuss the statistical distribution of $L\text{-}\alpha\text{-PMME}$.

Fig. 7 depicts the empirical CDFs and approximate CDFs of $L\text{-}\alpha\text{-PMME}$ under H_0 and H_1 , where Fig. 7(a) and Fig. 7(b) correspond to the case in which the number of samples is 50 and 1000, respectively. The results indicate that Gaussian distribution can well approximate the statistical distribution of $L\text{-}\alpha\text{-PMME}$ for the case of H_0 and H_1 . Resorting to this result, we assume that $L\text{-}\alpha\text{-PMME}$ approximately follows Gaussian distribution, i.e., $L\text{-}\alpha\text{-PMME} \sim \mathcal{N}(\mu_{L,H_i}^{H_i}, \sigma_{L,H_i}^2)$, $i = 0, 1$, in which $\mu_{L,H_i}^{H_i}$ and σ_{L,H_i}^2 represent the mean and variance of $L\text{-}\alpha\text{-PMME}$ under H_i , $i = 0, 1$.

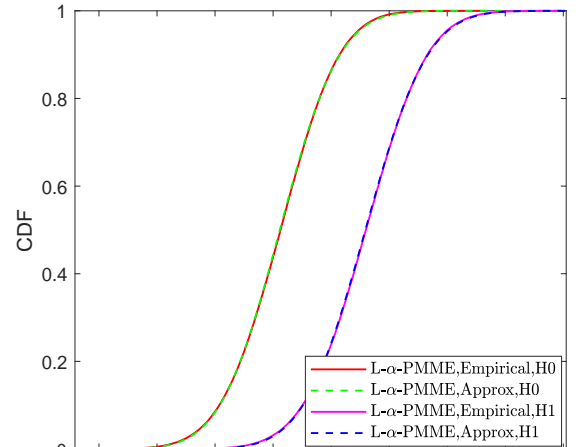
The P_{fa} , threshold and P_d of the $L\text{-}\alpha\text{-PMME}$ algorithm can be obtained using (26) and (30). On the basis of the relationship in (33), the P_{fa} , threshold and P_d of the α -PMME algorithm are further derived, which are expressed as

$$P_{fa}^{\text{PMME}} = Q\left(\frac{\eta_{\text{PMME}} - \mu_{\text{PMME}}^{H_0}}{\sigma_{\text{PMME},H_0}}\right), \quad (35)$$

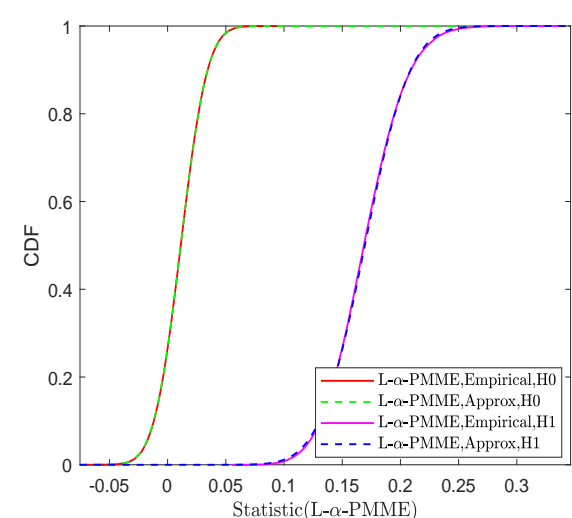
$$\eta_{\text{PMME}} = \exp\left(Q^{-1}(P_{fa}^{\text{PMME}}) \sigma_{\text{PMME},H_0} + \mu_{\text{PMME}}^{H_0}\right), \quad (36)$$

and

$$P_d^{\text{PMME}} = Q\left(\frac{\eta_{\text{PMME}} - \mu_{\text{PMME}}^{H_1}}{\sigma_{\text{PMME},H_1}}\right). \quad (37)$$



(a)



(b)

Fig. 7. Cumulative distribution functions for $L\text{-}\alpha\text{-PMME}$ under H_0 and H_1 . (a) $K = 50$. (b) $K = 1000$.

B. Analysis on Optimal Weight Coefficient α

The detection performance of the α -SMME and α -PMME algorithms closely depends on the weight coefficient α . In this subsection, the optimum weight selection for the α -SMME and α -PMME algorithms is discussed.

According to the Neyman-Pearson criterion, we require the P_d to be as high as possible under a given P_{fa} . Hence, the optimal weight α can be determined by solving the following optimization problem, which is written as

$$\begin{cases} \max_{\alpha} P_d(\eta, \alpha) \\ \text{s.t. } P_{fa}(\eta, \alpha) = p_0, \\ \quad 0 \leq \alpha \leq 1, \end{cases} \quad (38)$$

in which p_0 is the preset false alarm probability.

Here, we take the α -SMME algorithm as an example. Substituting (28) and (31) into (38), the optimization problem

is recast as

$$\left\{ \begin{array}{l} \max_{\alpha} Q \left(\frac{\eta_{SMME} - (\alpha \mu_{\lambda_1}^{H_1} + (1-\alpha) \mu_{\lambda_M}^{H_1})}{\sqrt{\alpha^2 \sigma_{\lambda_1, H_1}^2 + (1-\alpha)^2 \sigma_{\lambda_M, H_1}^2}} \right) \\ \text{s.t. } Q \left(\frac{\eta_{SMME} - (\alpha \mu_{\lambda_1}^{H_0} + (1-\alpha) \mu_{\lambda_M}^{H_0})}{\sqrt{\alpha^2 \sigma_{\lambda_1, H_0}^2 + (1-\alpha)^2 \sigma_{\lambda_M, H_0}^2}} \right) = p_0, \\ 0 \leq \alpha \leq 1. \end{array} \right. \quad (39)$$

For simplicity, the objective function is denoted as

$$g(\eta_{SMME}, \alpha) = Q \left(\frac{\eta_{SMME} - (\alpha \mu_{\lambda_1}^{H_1} + (1-\alpha) \mu_{\lambda_M}^{H_1})}{\sqrt{\alpha^2 \sigma_{\lambda_1, H_1}^2 + (1-\alpha)^2 \sigma_{\lambda_M, H_1}^2}} \right). \quad (40)$$

As observed from the first constraint in formula (39), the threshold η_{SMME} can be expressed as a function of α , which is given by

$$\eta_{SMME} = Q^{-1}(p_0) \sqrt{\alpha^2 \sigma_{\lambda_1, H_0}^2 + (1-\alpha)^2 \sigma_{\lambda_M, H_0}^2} + (\alpha \mu_{\lambda_1}^{H_0} + (1-\alpha) \mu_{\lambda_M}^{H_0}). \quad (41)$$

Substituting (41) into the equation (40), the objective function is recast as

$$g(\alpha) = Q \left(\frac{Q^{-1}(p_0) \sqrt{\alpha^2 \sigma_{\lambda_1, H_0}^2 + (1-\alpha)^2 \sigma_{\lambda_M, H_0}^2} + \alpha(\mu_{\lambda_1}^{H_0} - \mu_{\lambda_1}^{H_1}) + (1-\alpha)(\mu_{\lambda_M}^{H_0} - \mu_{\lambda_M}^{H_1})}{\sqrt{\alpha^2 \sigma_{\lambda_1, H_1}^2 + (1-\alpha)^2 \sigma_{\lambda_M, H_1}^2}} \right). \quad (42)$$

Since $Q(\cdot)$ is a monotonically decreasing function, maximizing the objective function in (42) is equivalent to minimizing the following function

$$\tilde{g}(\alpha) = \frac{Q^{-1}(p_0) \sqrt{\alpha^2 \sigma_{\lambda_1, H_0}^2 + (1-\alpha)^2 \sigma_{\lambda_M, H_0}^2} + \alpha(\mu_{\lambda_1}^{H_0} - \mu_{\lambda_1}^{H_1}) + (1-\alpha)(\mu_{\lambda_M}^{H_0} - \mu_{\lambda_M}^{H_1})}{\sqrt{\alpha^2 \sigma_{\lambda_1, H_1}^2 + (1-\alpha)^2 \sigma_{\lambda_M, H_1}^2}}. \quad (43)$$

The optimization problem in (39) is further transformed into

$$\left\{ \begin{array}{l} \min_{\alpha} \tilde{g}(\alpha) \\ \text{s.t. } 0 \leq \alpha \leq 1, \end{array} \right. \quad (44)$$

which is a convex optimization problem.

The derivative of the objective function $\tilde{g}(\alpha)$ with respect to α is expressed as that in (45).

$$\begin{aligned} \tilde{V}g(\alpha) &= Q^{-1}(p_0) \alpha(1-\alpha) \left(\sigma_{\lambda_1, H_0}^2 \sigma_{\lambda_M, H_1}^2 - \sigma_{\lambda_1, H_1}^2 \sigma_{\lambda_M, H_0}^2 \right) \\ &\quad + \sqrt{\alpha^2 \sigma_{\lambda_1, H_0}^2 + (1-\alpha)^2 \sigma_{\lambda_M, H_0}^2} \\ &\quad \times \left((1-\alpha)(\mu_{\lambda_M}^{H_0} - \mu_{\lambda_M}^{H_1}) \sigma_{\lambda_M, H_1}^2 - \alpha(\mu_{\lambda_1}^{H_0} - \mu_{\lambda_1}^{H_1}) \sigma_{\lambda_1, H_1}^2 \right). \end{aligned} \quad (45)$$

Let $\nabla \tilde{g}(\alpha) = 0$, a equation about α is given by (46).

Since the equation (46) is a high-order equation of α , it is difficult to give an analytical solution. Hence, the numerical solution is given through the toolbox in Matlab. In a similar way, the optimal weight of the α -PMME algorithm can be obtained.

The evaluations of the optimal α in the α -SMME and α -PMME algorithms are analyzed for different parameters, where the multipath channel order (C_{mp}), the number of primary users (P), the number of receiving antennas (M), the number of samples (N), and SNR are considered. Table III presents the optimal α of the two algorithms under the

condition that C_{mp} is 1, 2, and 4, M is 2 to 4, P is 2 to 4, N is 500, 1000, and 2000, as well as the SNR ranges from -20dB to -16dB with an interval of 2dB. It is worth noting that other parameters are fixed when analyzing the effect of a certain parameter on the evaluation of the optimal α . The results in Table III clearly show that the optimal α changes slightly for each parameter. For example, the optimal α of α -SMME is 0.5699 and 0.535 for the case of $C_{mp} = 1$ and $C_{mp} = 4$, and the optimal α of α -PMME is 0.5929 and 0.5775. The results indicate that the optimal weights of the two algorithms are not greatly affected by the changing channel conditions.

C. Computational Complexity Analysis

This subsection compares the computational complexity of the proposed algorithms and the typical algorithms based on extreme eigenvalues. The computational complexity includes the number of additions, multiplications, and exponential operations. Table IV summarizes the computational complexity for each algorithm. It is noted that the maximum eigenvalue and minimum eigenvalue are computed by the iterative power algorithm and shift power algorithm without computing all the eigenvalues, and the computational complexity of solving the extreme eigenvalues is $O(M^2)$ [35, 48-49]. Since the algorithms except MED include the computation of the maximum eigenvalue and minimum eigenvalue, the computational complexity is $2 \cdot O(M^2)$.

Besides, the time complexity of each algorithm is compared by recording the running time via a quad core i5 processor. As observed from Table IV, the complexity of the α -PMME and α -SMME algorithms is close to that of MME, MED, DMM and MSEE; the complexity of LRT is slightly higher, and the NB algorithm costs the highest complexity compared with other algorithms based on extreme eigenvalues.

V. SIMULATION RESULTS AND DISCUSSIONS

In this section, some simulation experiments are performed to analyze the performance of the proposed algorithms. The detailed parameter settings are as follows, unless otherwise stated, the number of PUs is $P = 3$; the number of antennas at received terminal is $M = 4$; the number of samples is $K = 1000$. The scenario with multipath fading channel is considered, where the channel order is $C_{mp} = 4$. It is assumed that noise and each component of multipath channel are circularly symmetric complex Gaussian variables with zero mean and unit variance. Moreover, we assume that the transmitted data is modulated with binary phase-shift keying constellation.

The detection performance of the α -PMME and α -SMME algorithms under different α is discussed through simulation experiments. Fig. 8(a) and Fig. 8(b) show the receiver operating characteristics (ROC) curves for the α -PMME and α -SMME algorithms under different α , where α takes a value between 0 and 1 with an interval of 0.1, SNR is set as -20dB, and P_{fa} varies from 10^{-3} to 1. The thresholds of the α -PMME and α -SMME algorithms are calculated using the analytic expressions in (29) and (36). The enlarged subfigures in Fig. 8(a) and Fig. 8(b) indicate that there exists an α

$$\alpha(1-\alpha) + \frac{\sqrt{\alpha^2\sigma_{\lambda_1,H_0}^2 + (1-\alpha)^2\sigma_{\lambda_M,H_0}^2}((1-\alpha)(\mu_{\lambda_M}^{H_0} - \mu_{\lambda_M}^{H_1})\sigma_{\lambda_M,H_1}^2 - \alpha(\mu_{\lambda_1}^{H_0} - \mu_{\lambda_1}^{H_1})\sigma_{\lambda_1,H_1}^2)}{Q^{-1}(p_0)(\sigma_{\lambda_1,H_0}^2\sigma_{\lambda_M,H_1}^2 - \sigma_{\lambda_1,H_1}^2\sigma_{\lambda_M,H_0}^2)} = 0. \quad (46)$$

TABLE III
OPTIMAL α OF THE α -SMME AND α -PMME ALGORITHMS UNDER DIFFERENT PARAMETERS

Optimal α -Parameters Algorithms	C_{mp}			M			P			N			SNR(dB)		
	1	2	4	2	3	4	2	3	4	500	1000	2000	-20	-18	-16
α -SMME	0.5699	0.5516	0.535	0.5174	0.5264	0.535	0.5531	0.535	0.5237	0.519	0.535	0.5422	0.535	0.5328	0.5026
α -PMME	0.5929	0.5898	0.5775	0.5344	0.5595	0.5775	0.5940	0.5775	0.5648	0.578	0.5775	0.5734	0.5775	0.5766	0.5576

TABLE IV
COMPLEXITY COMPARISON AMONG THE ALGORITHMS BASED ON EXTREME EIGENVALUES.

Name	MED [17]	MME [19]	DMM [30]	MSEE [34]	α -SMME	α -PMME	LRT	NB
Iterative/Shift power	$O(M^2)$	$2 \cdot O(M^2)$						
Multiplication	0	1	0	2	2	1	14	9
Addition	0	0	1	1	1	0	10	1
Exponential	0	0	0	1	0	2	0	2
Time (sec.)	0.0483	0.0627	0.0494	0.0525	0.0566	0.0712	0.2947	0.6761

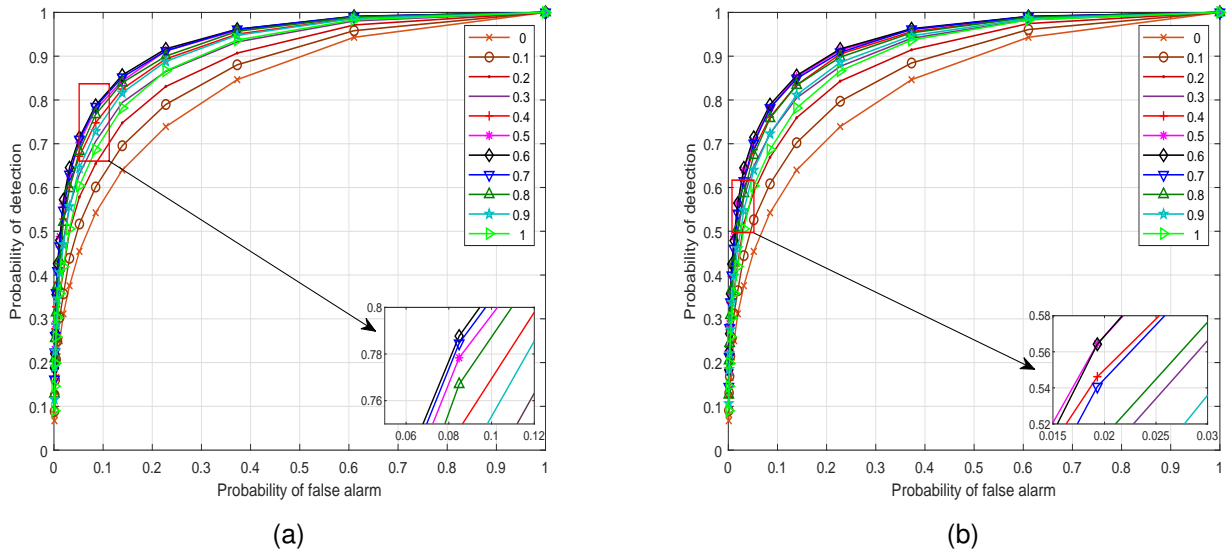


Fig. 8. ROC curves of the α -PMME and α -SMME algorithms for different α . (a) α -PMME. (b) α -SMME

corresponding to the optimal detection performance for the two algorithms. The optimal weights in the α -PMME and α -SMME algorithms are 0.6 and 0.5. Taking $P_{fa} = 0.01$ as an example, the optimal α of the two algorithms can be obtained by solving the optimization problem (38), which is 0.5858 and 0.5453, respectively. The experimental results almost coincide with the theoretical ones, which verifies the validity of theoretical analysis.

To evaluate the theoretical analysis on P_{fa} of the α -PMME and α -SMME methods, the theoretical thresholds are verified by simulation experiments, in which the values of α in the two algorithms are given by solving the optimization problem (38). The thresholds of the α -PMME and α -SMME algorithms are calculated by formulas (29) and (36). Fig. 9(a) and Fig. 9(b)

depict the theoretical P_{fa} and simulated P_{fa} of the α -PMME and α -SMME algorithms versus threshold. It can be clearly drawn from Fig. 9, the simulated P_{fa} perfectly coincides with the theoretical solutions, which demonstrates the effectiveness of the theoretical thresholds.

Under different SNRs, Fig. 10 makes a comparison for the detection probability of the proposed detectors and some typical detectors based on extreme eigenvalues. For comparison, the optimal eigenvalue weighted (OEW) detector designed using all eigenvalues in [50] is considered. The weight coefficients of the α -PMME and α -SMME algorithms respectively choose 0.5858 and 0.5453. SNR is set as $[-30, 0]$ dB, P_{fa} is 0.01. As shown in Fig. 10, the proposed algorithms achieve improvement over the MED, MME, DMM, and MSEE meth-

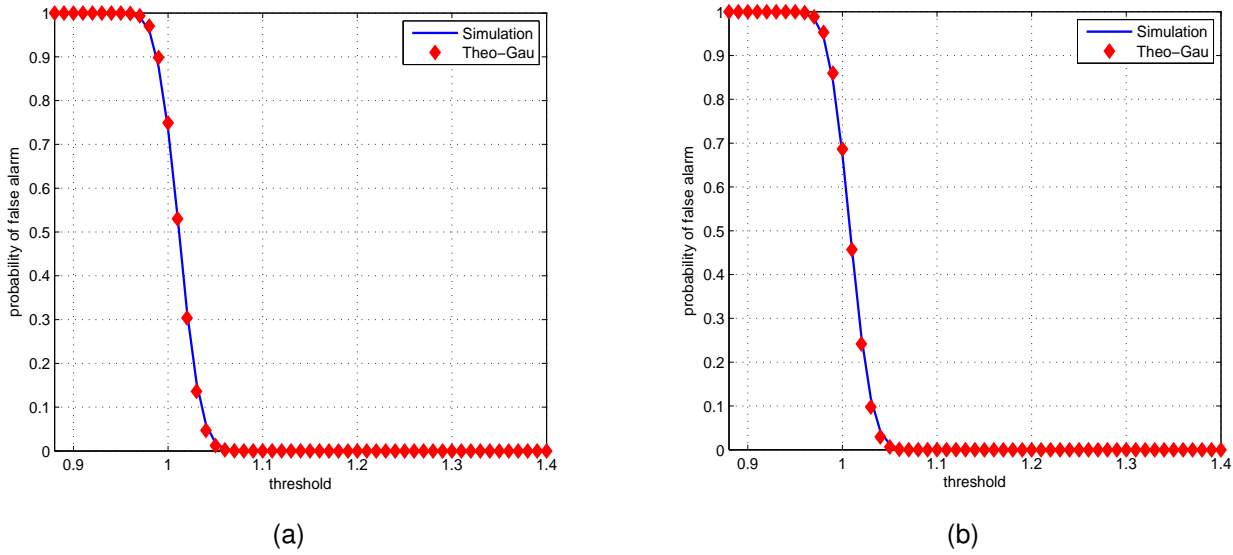


Fig. 9. Theoretical and simulated P_{fa} versus the thresholds of the α -PMME and α -SMME algorithms. (a) α -PMME. (b) α -SMME.

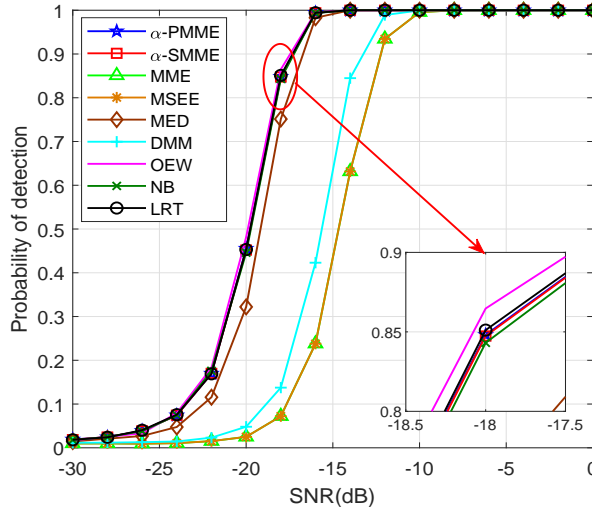


Fig. 10. Detection performance comparisons among the proposed detectors and some existing detectors using extreme eigenvalues.

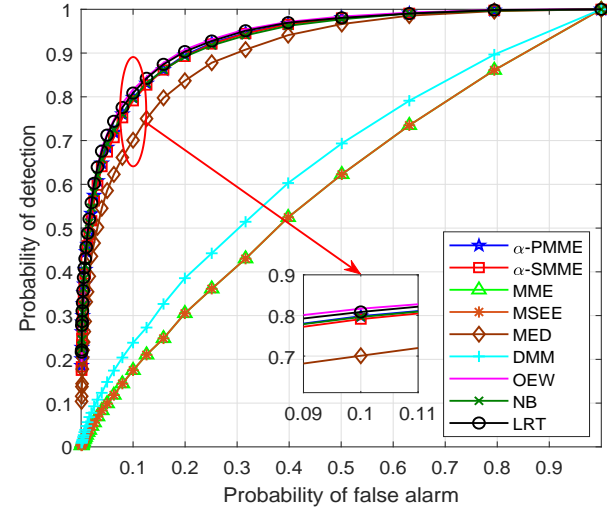


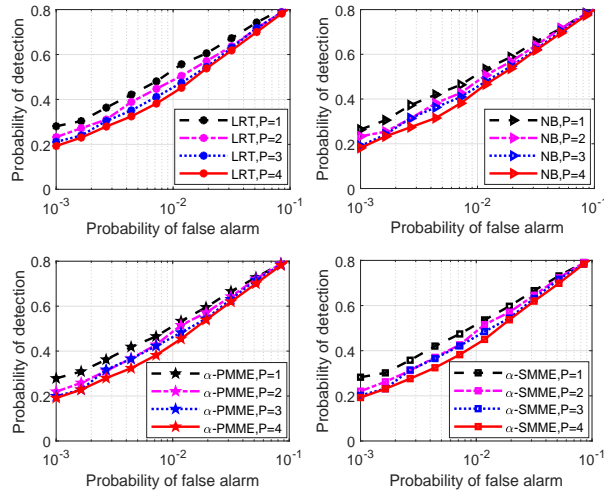
Fig. 11. ROC curve comparisons among the proposed algorithms and some existing algorithms using extreme eigenvalues.

ods, and the OEW algorithm has the optimal performance. However, the OEW algorithm relies on the PUs' signals, channel and noise information, which is infeasible in practical application scenarios [50]. The performance gaps among the proposed algorithms (NB, LRT, α -PMME and α -SMME) and the OEW algorithm are extremely narrow. Besides, the NB, α -PMME and α -SMME algorithms achieve almost the same performance as the LRT detector based on extreme eigenvalues.

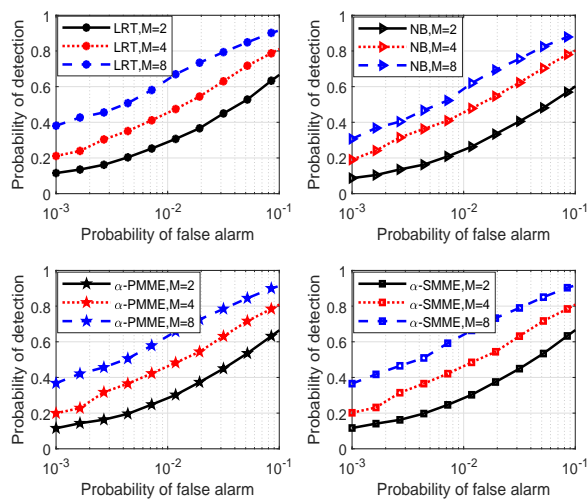
Fig. 11 plots the ROC curves of the LRT, NB, α -PMME, α -SMME, OEW, MED, MME, DMM and MSEE methods at $\text{SNR} = -20\text{dB}$. As shown in Fig. 11, the gaps among the optimal algorithms (OEW and LRT), α -PMME, α -SMME and NB algorithms are narrow. The P_d of the α -PMME, α -SMME and NB algorithms is superior to the MED, MME, DMM, and MSEE methods for any given P_{fa} . Taking $P_{fa} = 0.1$ as an example, the P_d of α -PMME and α -SMME achieves

approximately 62% and 60% improvement over the MSEE algorithm, respectively. It's worth noting that the performance gaps among the proposed methods and the existing methods are widening for low P_{fa} . Therefore, we conclude that the proposed algorithms are more suitable for practical applications.

Finally, we consider the influence of different values of P and M on the detection performance of the proposed detectors (LRT, NB, α -PMME and α -SMME). Fig. 12(a) plots the ROC curves of the proposed detectors for a range of P values, where P is set to 1 to 4. The results in Fig. 12(a) show that the detection performance of each detector is improved with the decrease of P . Fig. 12(b) shows the ROC curves of the proposed detectors under different number of receiving antennas, where M is set as 2, 4 and 8. As observed from Fig. 12(b), each detector achieves detection performance improvement as M increases due to the higher diversity gain resulted from increasing the number of receiving antenna.



(a)



(b)

Fig. 12. ROC curves of the proposed detectors under different values of P . (a) Detection performance under different values of P . (b) Detection performance under different values of M .

VI. CONCLUSION

This paper summarizes a unified framework for detector design via model-driven and data-driven approaches. The extreme eigenvalues based LRT detector is proposed using model-driven approach. The NB, α -SMME and α -PMME algorithms are designed by merging the model-driven and data-driven approaches. According to the Neyman-Pearson criterion, the optimal weights of the α -SMME and α -PMME algorithms are obtained by solving optimization problems. Besides, we apply the Gaussian approximation approach to derive the analytic expressions of P_d , P_{fa} and thresholds for the α -PMME and α -SMME algorithms. Simulation experiments verify that the theoretical thresholds of the α -PMME and α -SMME algorithms coincide with the simulated ones. Finally, simulation results demonstrate that the NB, α -PMME and α -SMME algorithms have distinct performance advantages over the state-of-the-art algorithms using extreme eigenvalues, and almost reach the performance of the LRT and OEW detectors.

Compared with the LRT and NB algorithms, α -PMME and α -SMME cost lower complexity.

APPENDIX

ANALYSIS OF DEPENDENCY BETWEEN λ_1 AND λ_M

The bivariate joint distribution function $F_{\lambda_1, \lambda_M}(a, b) = P_r\{\lambda_1 \leq a, \lambda_M \leq b\}$ of λ_1 and λ_M can be represented by a Copula C , which is defined as follows [51],

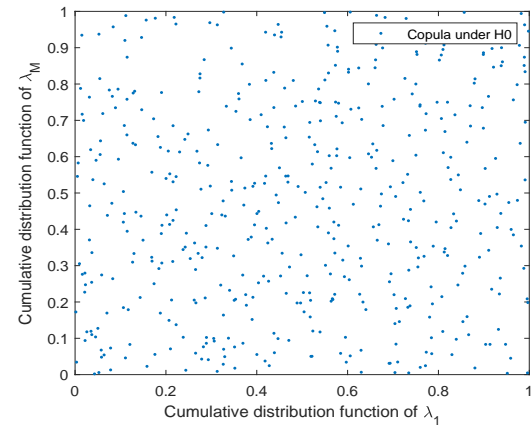
$$F_{\lambda_1, \lambda_M}(a, b) = C(F_{\lambda_1}(a), F_{\lambda_M}(b)) \stackrel{\Delta}{=} C(u, v), \quad (47)$$

where $u = F_{\lambda_1}(a) = P_r\{\lambda_1 \leq a\}$, and $v = F_{\lambda_M}(b) = P_r\{\lambda_M \leq b\}$.

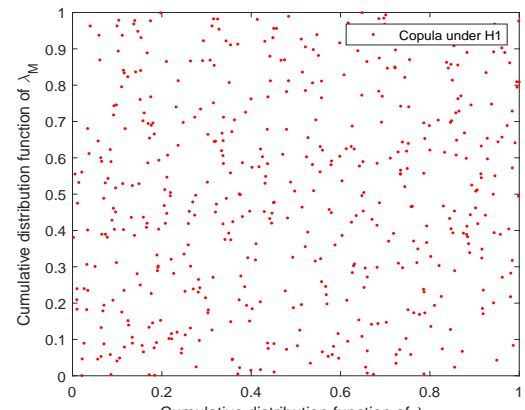
Furthermore, Copula is given by [47],

$$C(u, v) = F_{\lambda_1, \lambda_M}(F_{\lambda_1}^{-1}(u), F_{\lambda_M}^{-1}(v)). \quad (48)$$

Copula represents the multidimensional functions that link marginal PDFs of random variables to joint PDF, which provides a detailed description of the dependency structure between two random variables [52].



(a)



(b)

Fig. 13. Copula distributions of λ_1 and λ_M under H_0 and H_1 . (a) H_0 . (b) H_1 .

Fig. 13(a) and Fig. 13(b) respectively show the Copula between λ_1 and λ_M under H_0 and H_1 . In each case, the Copula distribution resorts to the empirical CDFs of the two random variables. It can be seen clearly that the structure for the Copula distribution of λ_1 and λ_M is non-distinctive under

H_0 and H_1 , which shows that λ_1 and λ_M are independent; otherwise, the distributions are distinctive in case if the random variables are correlated [47].

ACKNOWLEDGMENTS

The authors would like to thank the reviewers and handling editor for their constructive comments, notes, and suggestions.

REFERENCES

- [1] J. A. Ansere, G. Han, H. Wang, C. Choi, and C. Wu, "A reliable energy efficient dynamic spectrum sensing for cognitive radio IoT networks," *IEEE Internet Things J.*, vol. 6, no. 4, pp. 6748-6759, Aug. 2019.
- [2] Y. Huo, X. Dong, W. Xu, and M. Yuen, "Enabling multi-functional 5G and beyond user equipment: A survey and tutorial," *IEEE Access*, vol. 7, pp. 116975-117008, Aug. 2019.
- [3] M. Anjad, M. H. Rehmani, and S. Mao, "Wireless multimedia cognitive radio networks: A comprehensive survey," *IEEE Commun. Surv. Tutor.*, vol. 20, no. 2, pp. 1056-1103, Second Quarter, 2018.
- [4] W. Gardner, "Spectral correlation of modulated signals: Part I-analog modulation," *IEEE Trans. Commun.*, vol. 35, no. 6, pp. 5081-5096, Jun. 1987.
- [5] F. F. Digham, M. S. Alouini, and M. K. Simon, "On the energy detection of unknown signals over fading channels," *IEEE Trans. Commun.*, vol. 55, no. 1, pp. 21-24, Jan. 2007.
- [6] S. Bae, J. So, and H. Kim, "On optimal cooperative sensing with energy detection in cognitive radio," *Sensors.*, vol. 17, no. 9, pp. 1-15, Sep. 2017.
- [7] Y. Ye, Y. Li, G. Lu, and F. Zhou, "Improved energy detection with Laplacian noise in cognitive radio," *IEEE Syst. J.*, vol. 13, no. 1, pp. 18-29, Mar. 2019.
- [8] S. Dikmese, P. C. Sofotasios, M. Renfors, and M. Valkama, "Subband energy based reduced complexity spectrum sensing under noise uncertainty and frequency-selective spectral characteristics," *IEEE Trans. Signal Process.*, vol. 64, no. 1, pp. 131-145, Jan. 2016.
- [9] A. Gokceoglu, S. Dikmese, M. Valkama, and M. Renfors, "Energy detection under IQ imbalance with single-and multi-channel direct-conversion receiver: Analysis and mitigation," *IEEE J. Sel. Areas Commun.*, vol. 32, no. 3, pp. 411-424, Mar. 2014.
- [10] A. Mehrabian and A. Zaimbashi, "Spectrum sensing in SIMO cognitive radios under primary user transmitter IQ imbalance," *IEEE Syst. J.*, vol. 13, no. 2, pp. 1210-1218, Jun. 2019.
- [11] A. Mehrabian and A. Zaimbashi, "Robust and blind eigenvalue-based multiantenna spectrum sensing under IQ imbalance," *IEEE Trans. Wireless Commun.*, vol. 17, no. 8, pp. 5581-5591, Aug. 2018.
- [12] C. Guo, M. Jin, Q. Guo, and Y. Li, "Antieigenvalue-based spectrum sensing for cognitive radio," *IEEE Wirel. Commun. Lett.*, vol. 8, no. 2, pp. 544-547, Apr. 2019.
- [13] Y. Zeng and Y.-C. Liang, "Spectrum-sensing algorithms for cognitive radio based on statistical covariance," *IEEE Trans. Veh. Technol.*, vol. 58, no. 4, pp. 1804-1815, May 2009.
- [14] M. Jin, Y. Li, and H. G. Ryu, "On the performance of covariance based spectrum sensing for cognitive radio," *IEEE Trans. Signal Process.*, vol. 60, no. 7, pp. 3670-3682, Jul. 2012.
- [15] A. Bishnu and V. Bhatia, "Logdet covariance-based spectrum sensing under colored noise," *IEEE Trans. Veh. Technol.*, vol. 67, no. 7, pp. 6716-6720, Jul. 2018.
- [16] T. M. Getu, W. Ajib, and R. Landry, "Simple F-test-based spectrum sensing techniques for multi-antenna cognitive radios," *IEEE Trans. Commun.*, vol. 66, no. 11, pp. 5081-5096, Nov. 2018.
- [17] Y. Zeng, C. L. Koh, and Y.-C. Liang, "Maximum eigenvalue detection: Theory and application," in *Proc. IEEE Int. Conf. Commun.*, Beijing, China, May 2008, pp. 4160-4164.
- [18] Y. Zeng, Y.-C. Liang, A. T. Hoang, and R. Zhang, "A review on spectrum sensing for cognitive radio: Challenges and solutions," *EURASIP J. Adv. Signal Process.*, vol. 2010, no. 1, pp. 1-15, Jan. 2010.
- [19] Y. Zeng and Y.-C. Liang, "Eigenvalue-based spectrum sensing algorithms for cognitive radio," *IEEE Trans. Commun.*, vol. 57, no. 6, pp. 1784-1793, Jun. 2009.
- [20] A. Ali and W. Hamouda, "Advances on spectrum sensing for cognitive radio networks: Theory and applications," *IEEE Commun. Surv. Tutor.*, vol. 19, no. 2, pp. 1277-1304, Second Quarter, 2017.
- [21] F. Awin, E. Abdel-Raheem, and K. Tepe, "Blind spectrum sensing approaches for interweaved cognitive radio system: A tutorial and short course," *IEEE Commun. Surv. Tutor.*, vol. 21, no. 1, pp. 238-259, First Quarter, 2019.
- [22] P. Bianchi, M. Debbah, M. Maida, and J. Najim, "Performance of statistical tests for single-source detection using random matrix theory," *IEEE Trans. Inform. Theory.*, vol. 57, no. 4, pp. 2400-2419, Apr. 2011.
- [23] P. Wang, J. Fang, N. Han, and H. Li, "Multiantenna-assisted spectrum sensing for cognitive radio," *IEEE Trans. Veh. Technol.*, vol. 59, no. 4, pp. 1791-1800, May 2010.
- [24] B. Nadler, F. Penna, and R. Garello, "Performance of eigenvalue-based signal detectors with known and unknown noise level," in *Proc. IEEE Int. Conf. Commun.*, Kyoto, Japan, Jun. 2011, pp. 1-5.
- [25] T. J. Lim, R. Zhang, Y.-C. Liang, and Y. Zeng, "GLRT-based spectrum sensing for cognitive radio," in *Proc. IEEE Global Telecommun. Conf.*, New Orleans, LA, USA, Nov. 2008, pp. 1-5.
- [26] R. Zhang, T. J. Lim, Y.-C. Liang, and Y. Zeng, "Multi-antenna based spectrum sensing for cognitive radios: A GLRT approach," *IEEE Trans. Commun.*, vol. 58, no. 1, pp. 84-88, Jan. 2010.
- [27] N. Pillay and H. Xu, "Blind eigenvalue-based spectrum sensing for cognitive radio network," *IET Commun.*, vol. 6, no. 11, pp. 1388-1396, Jul. 2012.
- [28] W. Zhao, H. Li, M. Jin, Y. Liu, and S. J. Yoo, "Eigenvalues-based universal spectrum sensing algorithm in cognitive radio networks," *IEEE Syst. J.*, Early access.
- [29] S. Ali, C. Liu, and M. Jin, "Minimum eigenvalue detection for spectrum sensing in cognitive radio," *Inter. J. Electron. Computer Eng.*, vol. 4, no. 4, pp. 623-630, Aug. 2014.
- [30] A. Bollig and R. Mathar, "MMME and DME: Two new eigenvalue based detectors for spectrum sensing in cognitive radio," in *Proc. IEEE Global Conf. Signal, Information Process.*, Austin, TX, Dec. 2013, pp. 1210-1213.
- [31] R. B. Chaurasiya and R. Shrestha, "Hardware-efficient and fast sensing-time maximum-minimum-eigenvalue-based spectrum sensor for cognitive radio network," *IEEE Trans. Circuits Syst. I-Regul. Pap.*, vol. 66, no. 11, pp. 4448-4461, Nov. 2019.
- [32] W. Zhang, G. Abreu, M. Inamori, and Y. Sanada, "Spectrum sensing algorithms via finite random matrices," *IEEE Trans. Commun.*, vol. 60, no. 1, pp. 164-175, Jan. 2012.
- [33] W. Zhang, J. Wang, J. Sun, C. X. Wang, and X. Ge, "Standard condition number distributions of finite Wishart matrices for cognitive radio networks," *IEEE Trans. Veh. Technol.*, vol. 67, no. 5, pp. 4630-4634, May 2018.
- [34] K. Bouallegue, I. Dayoub, M. Gharbi, and K. Hassan, "Blind spectrum sensing using extreme eigenvalues for cognitive radio networks," *IEEE Commun. Lett.*, vol. 22, no. 7, pp. 1386-1389, Jul. 2018.
- [35] R. B. Chaurasiya and R. Shrestha, "Fast sensing-time and hardware-efficient eigenvalue-based blind spectrum sensors for cognitive radio network," *IEEE Trans. Circuits Syst. I, Reg. Papers*, vol. 67, no. 4, pp. 1296-1308, Apr. 2020.
- [36] D. Gündüz, P. de Kerret, N. D. Sidiropoulos, D. Gesbert, C. R. Murthy, and M. van der Schaaf, "Machine learning in the air," *IEEE J. Sel. Areas Commun.*, vol. 37, no. 10, pp. 2184-2199, Oct. 2019.
- [37] Z. Xu and J. Sun, "Model-driven deep-learning," *Natl. Sci. Rev.*, vol. 5, no. 1, pp. 22-24, Jan. 2018.
- [38] Z. Li, D. Wang, P. Qi, and B. Hao, "Maximum-eigenvalue-based sensing and power recognition for multiantenna cognitive radio system," *IEEE Trans. Veh. Technol.*, vol. 65, no. 10, pp. 8218-8229, Oct. 2016.
- [39] A. Zanella, M. Chiani, and M. Z. Win, "On the marginal distribution of the eigenvalues of Wishart matrices," *IEEE Trans. Commun.*, vol. 57, no. 4, pp. 1050-1060, Apr. 2009.
- [40] M. Chiani, M. Z. Win, and A. Zanella, "On the capacity of spatially correlated MIMO Rayleigh-fading channels," *IEEE Trans. Inf. Theory.*, vol. 49, no. 10, pp. 2363-2371, Oct. 2003.
- [41] F. Zhou and N. C. Beaulieu, "An improved and more accurate expression for a PDF related to eigenvalue-based spectrum sensing," *IEEE Syst. J.*, vol. 13, no. 2, pp. 1320-1323, Jun. 2019.
- [42] M. Z. Shakir, A. Rao, and M. S. Alouini, "On the decision threshold of eigenvalue ratio detector based on moments of joint and marginal distributions of extreme eigenvalues," *IEEE Trans. Wireless Commun.*, vol. 12, no. 3, pp. 974-983, Mar. 2013.
- [43] T. M. Mitchell, "Machine learning," 1st edition, New York, NY, USA: McGraw-Hill Inc., 1997.
- [44] S. M. Kay, "Fundamentals of statistical signal processing, Vol. II: Detection Theory," Prentice Hall PTR, Upper Saddle River, NJ, USA, 1998.

- [45] I. Sobron, P. S. R. Diniz, W. A. Martins, and M. Velez, "Energy detection technique for adaptive spectrum sensing," *IEEE Trans. Commun.*, vol. 63, no. 3, pp. 617-627, Mar. 2015.
- [46] B. Picinbono, "On deflection as a performance criterion in detection," *IEEE Trans. Aerosp. Electron. Syst.*, vol. 31, no. 3, pp. 1072-1081, Jul. 1995.
- [47] M. Z. Shakir, A. Rao, and M. S. Alouini, "Generalized mean detector for collaborative spectrum sensing," *IEEE Trans. Commun.*, vol. 61, no. 4, pp. 1242-1253, Apr. 2013.
- [48] S. Yousef, "Numerical methods for large eigenvalue problems," Philadelphia, PA, USA: SIAM, 2011.
- [49] J. W. Demmel, "Applied numerical linear algebra," Philadelphia, PA, USA: SIAM, 1997.
- [50] C. Liu, H. Li, J. Wang, and M. Jin, "Optimal eigenvalue weighting detection for multi-antenna cognitive radio networks," *IEEE Trans. Wireless Commun.*, vol. 16, no. 4, pp. 2083-2096, Apr. 2017.
- [51] T. S. Durrani and X. Zeng, "Copulas for bivariate probability distributions," *IET Electron. Lett.*, vol. 43, no. 4, pp. 248-249, Feb. 2007.
- [52] R. B. Nelsen, "An introduction of copulas," 2nd edition, Springer Science & Business Media, New York, USA, 2006.



Wenjing Zhao received the B.S. degree in mathematics and applied mathematics from Liaoning Normal University, Liaoning, China, in 2012, the M.S. degree in fundamental mathematics from Northeast Normal University, Changchun, China, in 2015, the Ph.D. degree in the School of Information and Communication Engineering from Dalian University of Technology, Dalian, China, in 2020. She is currently a Postdoctoral Research Fellow with the School of Information and Communication Engineering, University of Electronic Science and Technology of China, Chengdu, China. Her current research interests include information geometry, statistical signal processing, spectrum sensing in cognitive radio, and radar target detection.



Syed Sajjad Ali received the B.S. degree from the University of Karachi, Pakistan, the M.S. degree from the Mohammed Ali Jinnah University Karachi, Pakistan, the Ph.D. degree from School of Information and Communication Engineering, Dalian University of Technology, Dalian, China, in 2020. His research interests include wireless communication and signal processing for wireless communication system.



Minglu Jin (M'96) received the B.S. degree from the University of Science and Technology of China, Hefei, China, in 1982, the M.S. and Ph.D. degrees from Beijing University of Aeronautics and Astronautics, Beijing, China, in 1984 and 1995, respectively. He was a visiting scholar in the Ari-moto Laboratory, Osaka University, Osaka, Japan, from 1987 to 1988. He was a Research Fellow in Radio and Broadcasting Research Laboratory, Electronics Telecommunications Research Institute, Daejeon, South Korea, from 2001 to 2004. He is currently a Professor at Dalian University of Technology, Dalian, China. His research interests include wireless communication, wireless sensor networks, and signal processing for wireless communication system.



Guolong Cui (M'12-SM'17) received the B.S., M.S., and Ph.D. degrees from University of Electronic Science and Technology of China (UESTC), Chengdu, in 2005, 2008, and 2012, respectively. From June 2012 to August 2013, he was a postdoctoral researcher in the Department of Electrical and Computer Engineering, Stevens Institute of Technology, Hoboken, NJ. He joined UESTC in 2013 and is currently a Professor there. His current research interests include cognitive radar, array signal processing, MIMO radar and through the wall radar.



Young Researcher Award in 2018.

Nan Zhao (Senior Member, IEEE) is currently a Professor at Dalian University of Technology, China. He received the Ph.D. degree in information and communication engineering in 2011, from Harbin Institute of Technology, Harbin, China. Dr. Zhao is serving on the editorial boards of IEEE Wireless Communications and IEEE Wireless Communications Letters. He won the best paper awards in IEEE VTC 2017 Spring, ICNC 2018, WCSP 2018 and WCSP 2019. He also received the IEEE Communications Society Asia Pacific Board Outstanding



Sang-Jo Yoo (Member, IEEE) received the B.S. degree in electronic communication engineering from Hanyang University, Seoul, South Korea, in 1988, and the M.S. and Ph.D. degrees in electrical engineering from the Korea Advanced Institute of Science and Technology, in 1990 and 2000, respectively. From 1990 to 2001, he was a Member of Technical Staff with the Korea Telecom Research and Development Group, where he has been involved in communication protocol conformance testing and network design fields. From 1994 to 1995 and from 2007 to 2008, he was a Guest Researcher with the National Institute Standards and Technology, USA. Since 2001, he has been with Inha University, where he is currently a Professor with the Information and Communication Engineering Department. His current research interests include cognitive radio network protocols, adhoc wireless network MAC and routing protocol design, wireless network QoS, and wireless sensor networks.